Supporting Information

Coherent Arrangement of Perylene Diimide Derivative via Adhesion-Controlled Transfer for Noise-Suppressed Light Signal Detection

*Jihyun Lim[a], Woongsik Jang[b] Zhao Yang[b] and Dong Hwan Wang[a,b,]**

[a.]Department of Intelligent Semiconductor Engineering, Chung-Ang University, 84 Heukseok-ro, Dongjak-gu, Seoul 06974, Republic of Korea

[b.]School of Integrative Engineering, Chung-Ang University, 84 Heukseok-ro, Dongjak -gu, Seoul 06974, Republic of Korea

E-mail: king0401@cau.ac.kr

- **Functionalized Polymer Delamination Substrate Fabrication for coherent arrangement Assembly NPDI**

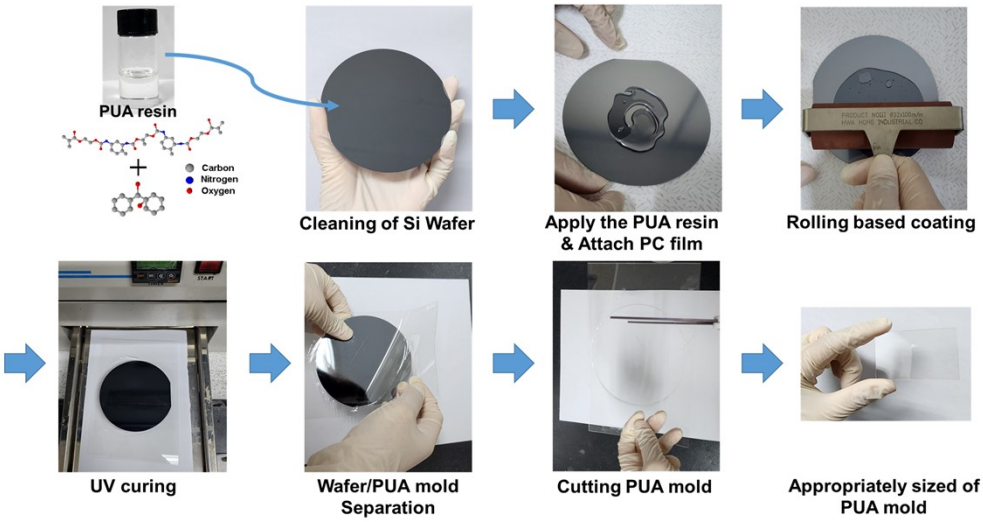

Fig. S1. Mold fabrication process for the coherent arrangement assembly of NPDI

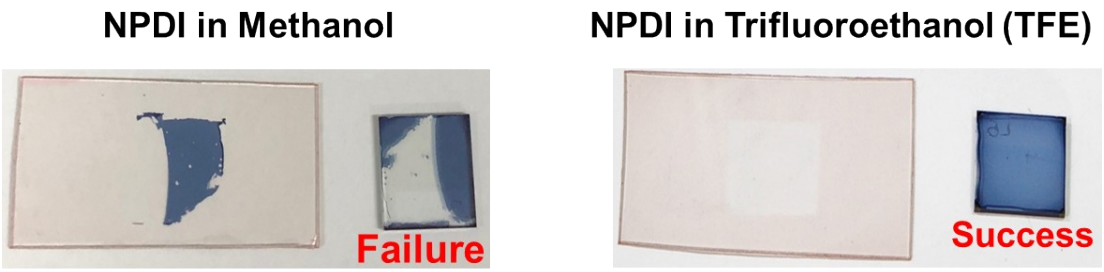

Fig. S2. Photographic images of the formation of the coherent arrangement of NPDI layers using methanol or trifluoroethanol (TFE) as the solvent.

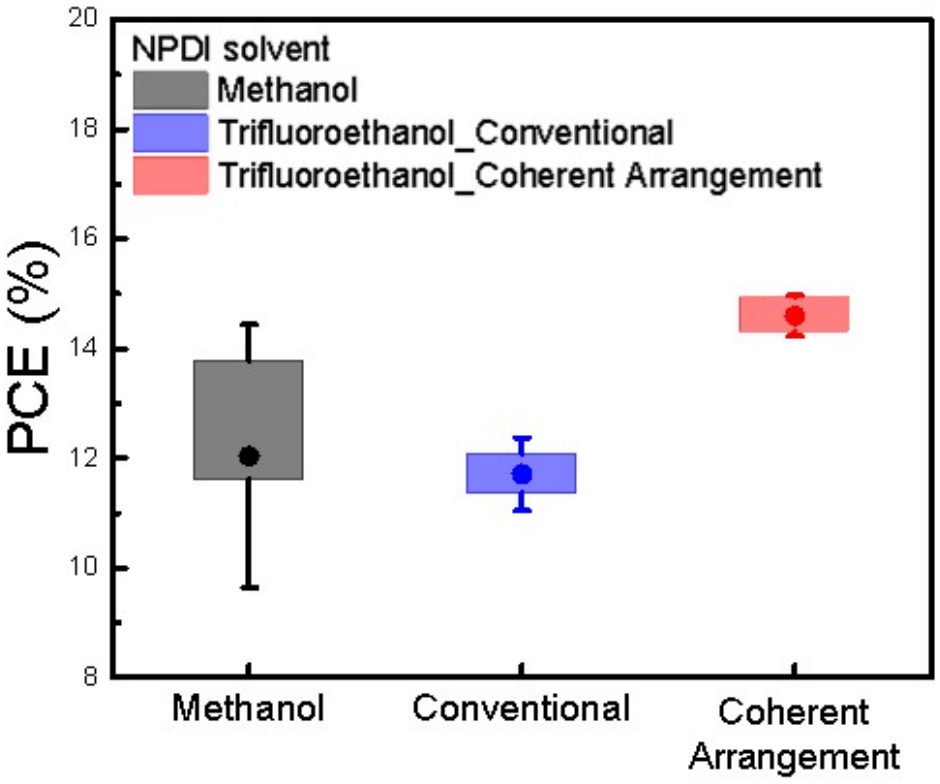

Fig. S3. PCE of the NPDI electron transport layer with methanol or trifluoroethanol as the solvent

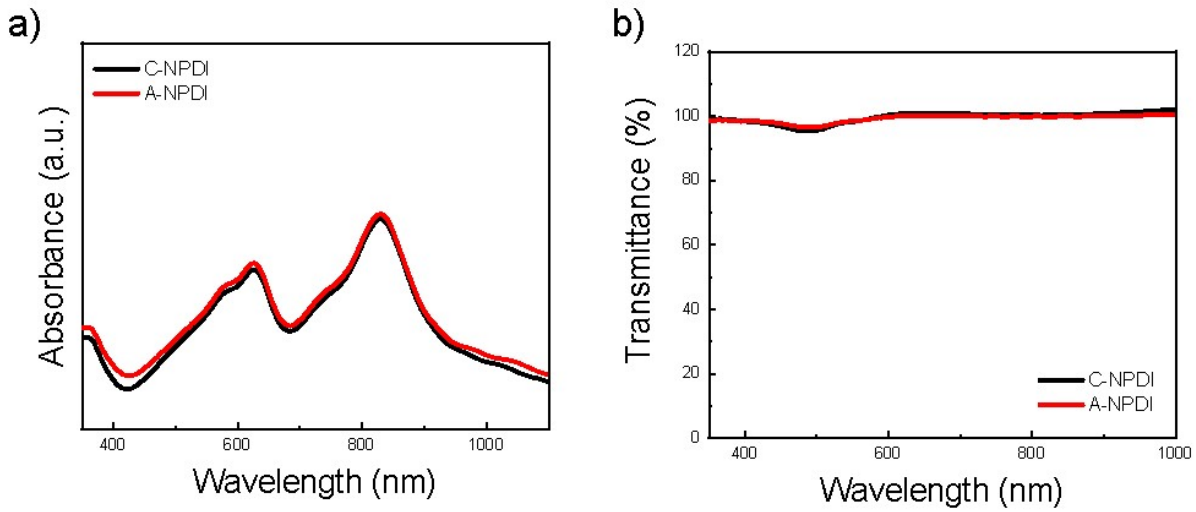

Fig. S4. (a) UV−visible absorbance spectra and (b) transmittance analysis for PEDOT:PSS/PM6:Y12/NPDI devices with coherent arrangement of NPDI (red line) and conventional NPDI (black line).

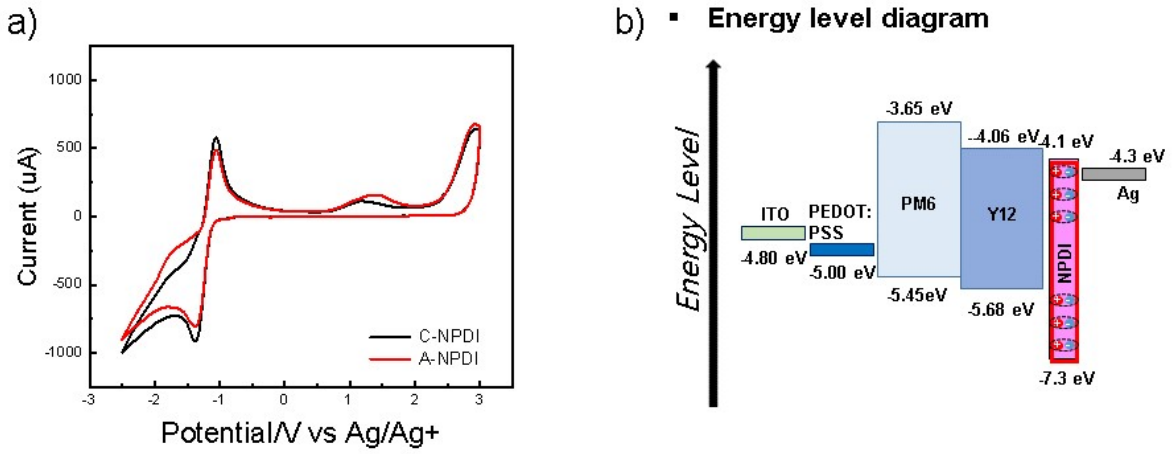

Fig. S5. Cyclic voltammetry analysis of coherent arrangement of NPDI (red line) and conventional NPDI (black line). (b) Energy level diagram of the device.

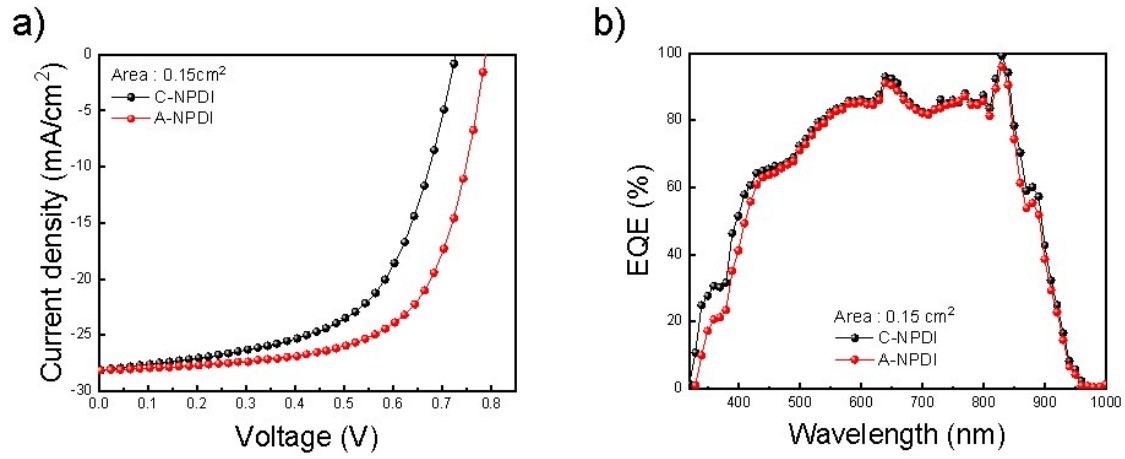

Fig. S6. (a) Current density−voltage curves under illumination (100 mW/cm^2) and (b) EQE spectra for PEDOT:PSS/PM6:Y12/NPDI devices with a coherent arrangement of NPDI (red line) and conventional NPDI (black line) (Area: 0.15 cm^2).

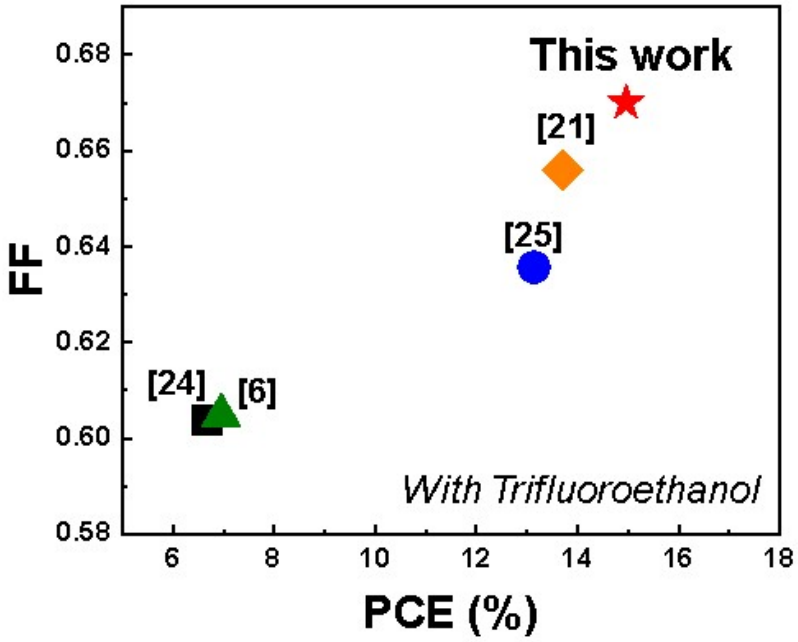

Fig. S7. Chart of reported FF and PCE for non-fullerene acceptor based organic photovoltaic devices with 2,2,2- trifluoroethanol.

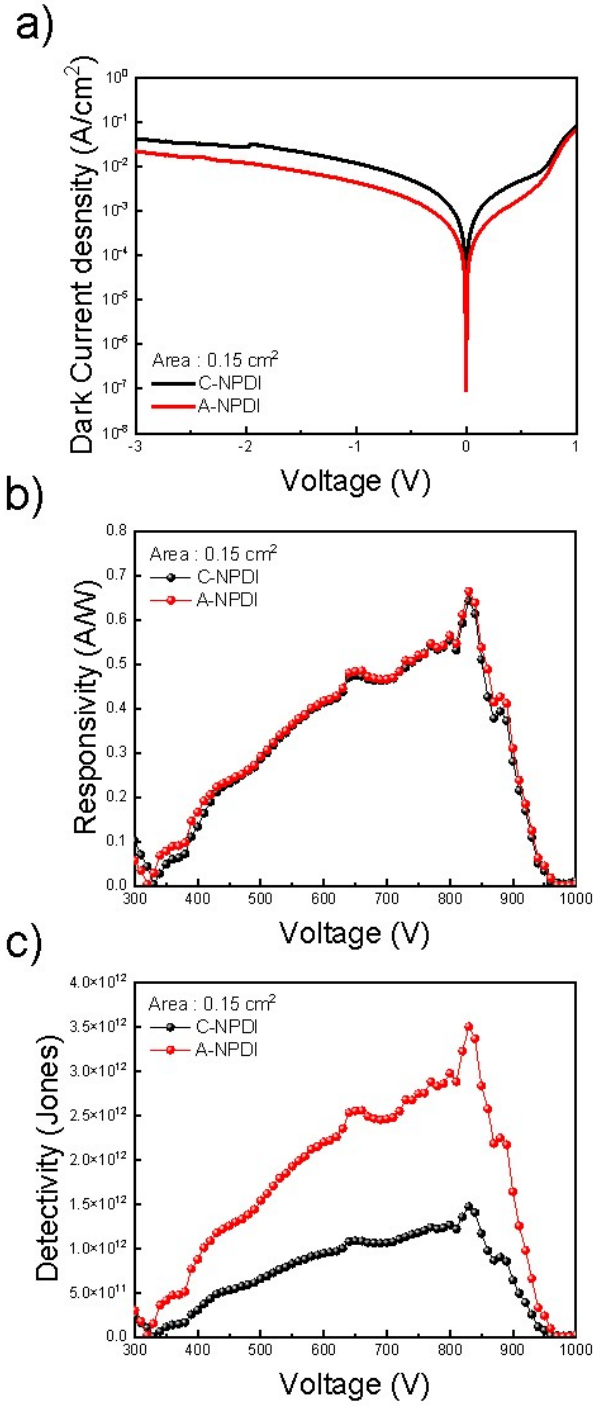

Fig. S8. (a) Dark current density−voltage curves, (b) responsivity at 0 V, and (c) detectivity at 0 V for an area of 0.15 cm^2 for OPD devices with a coherent arrangement NPDI (red line) and conventional NPDI (black line).

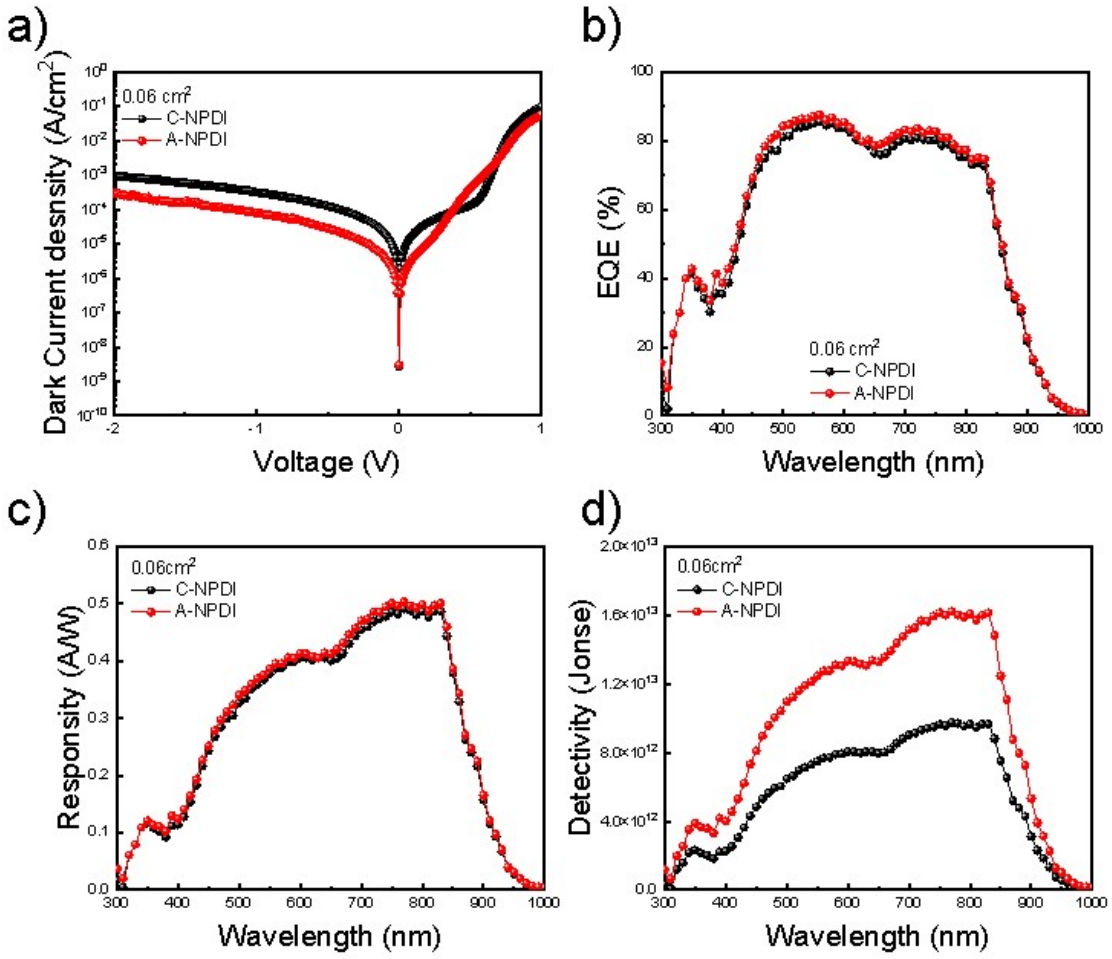

Fig. S9. (a) Dark current density−voltage curves, (b) EQE, (c) responsivity at 0 V, and (d) detectivity at 0 V for an area of 0.06 cm^2 for OPD devices with a coherent arrangement NPDI (red line) and conventional NPDI (black line).

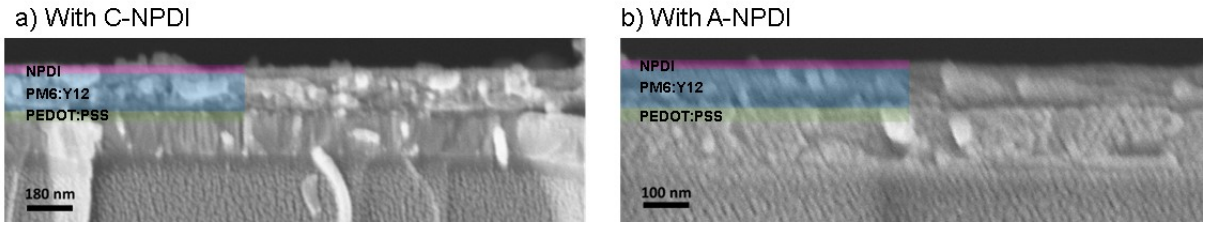

Fig. S10. FE-SEM cross-sections of PEDOT:PSS/PM6:Y12/NPDI devices with (a) conventional NPDI and (b) coherent arrangement NPDI.

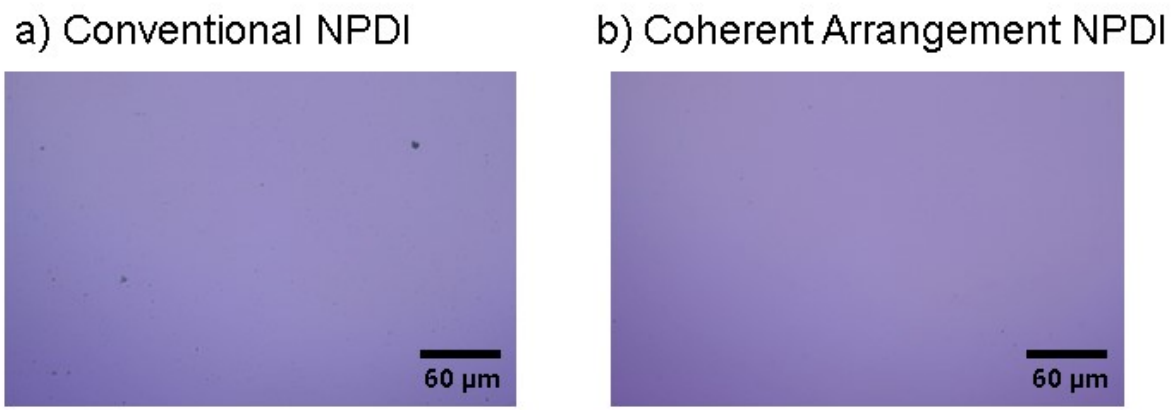

Fig. S11. Optical microscopic images of (a) conventional NPDI and (b) coherent arrangement of NPDI films.

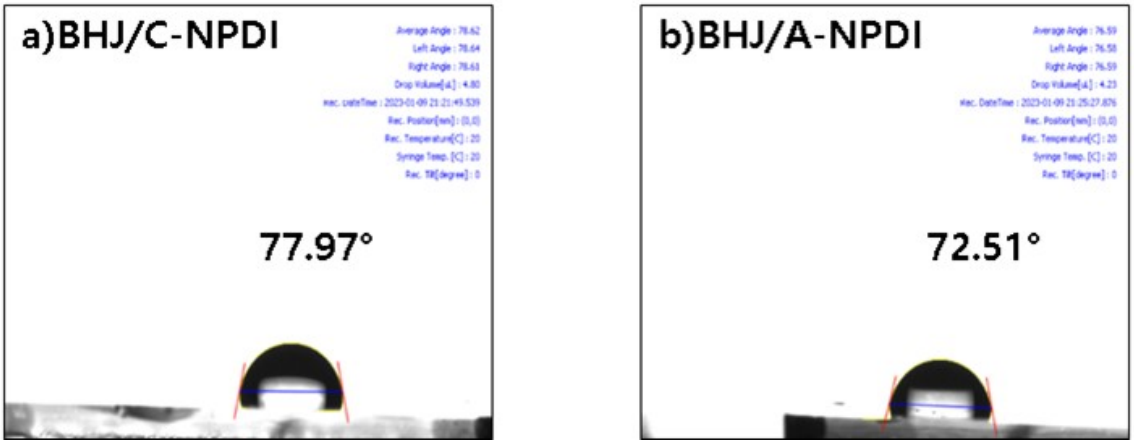

Fig. S12. DI water contact angle analysis of BHJ with (a) conventional NPDI and (b) coherent arrangement NPDI films.

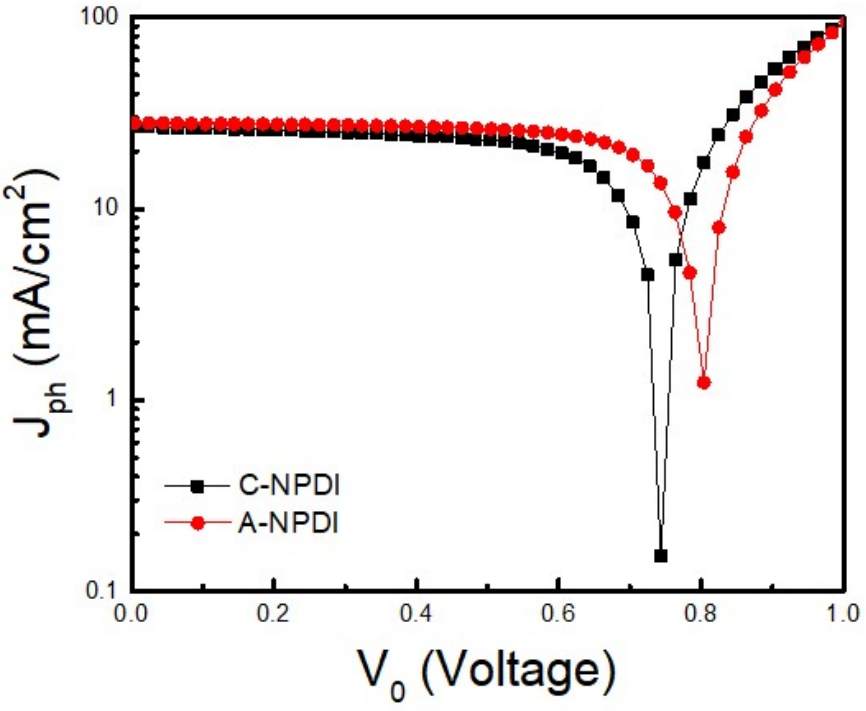

Fig. S13. Compensation voltages under illumination of C-NPDI based device and A-NPDI based device.

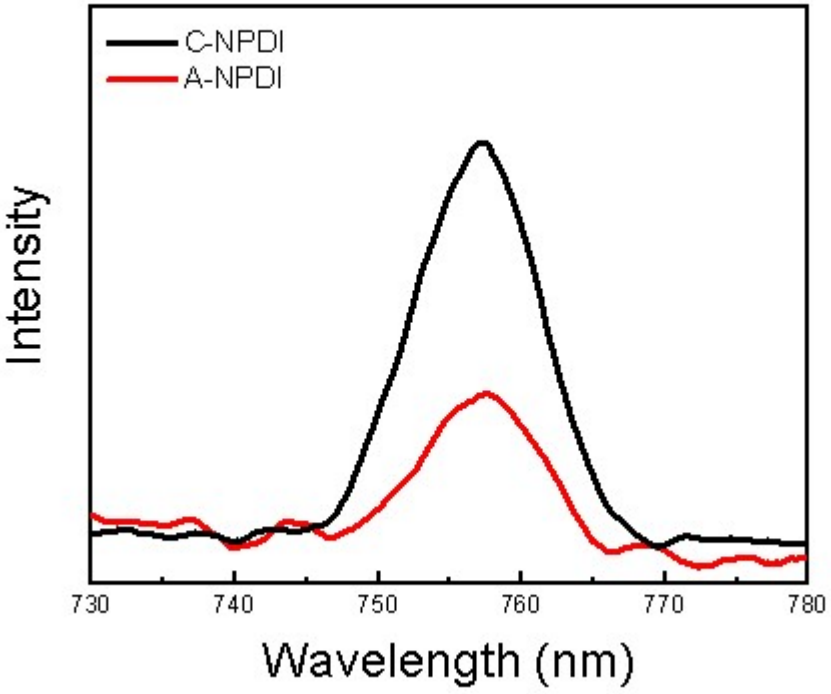

Fig. S14. Photoluminescence analysis of ITO/PEDOT:PSS/PM6:Y12/NPDI devices with coherent arrangement NPDI (red line) and conventional NPDI (black line),

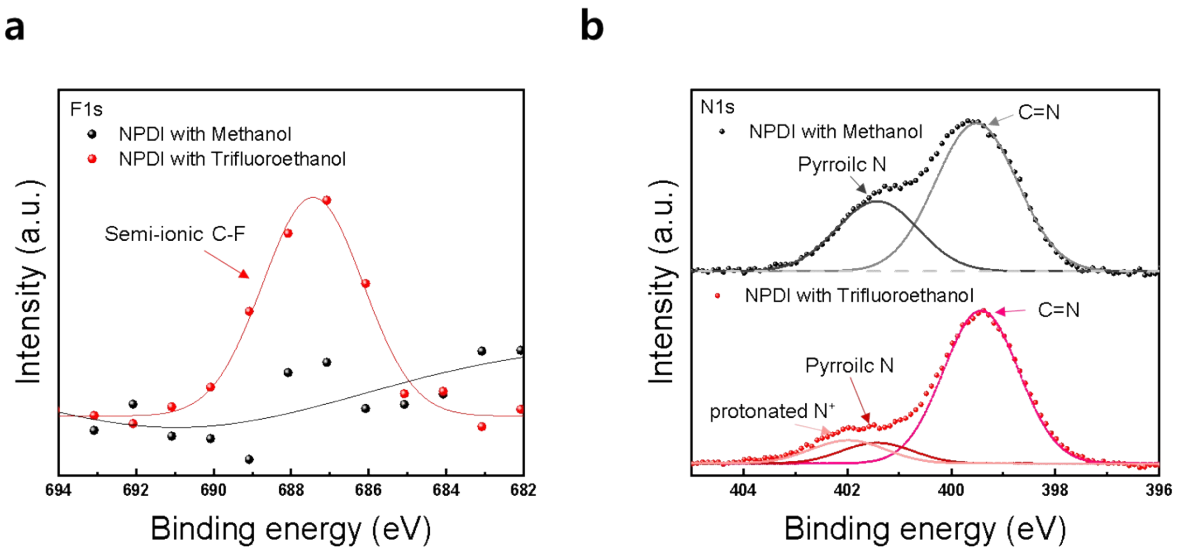

Fig. S15. XPS survey spectra of the atomic core levels for the NPDI with methanol and trifluoroethanol; a) F1s, b) N1s.

Table S1. Surface energy parameters for various films.

Material		γ_{SV} (mJ/m^2)	γ_{SV}^{p} (mJ/m^2)	γ_{SV}^{d} (mJ/m^2)
PUA		55.66	46.12	9.53
BHJ (PM6:Y12)		34.11	31.87	2.23
NPDI	**Methanol**	76.15	40.99	35.16
	Trifluoroethanol	77.30	43.75	33.55

Table S2. Calculated interfacial surface energy for NPDI, BHJ, and PUA.

PM6:Y12	Material	Interfacial energy [mJ m^{-2}]
	PUA	3.87
NPDI with methanol	PUA	8.23
	PM6:Y12	20.26
NPDI with trifluoroethanol	PUA	7.35
	PM6:Y12	19.43

Table S3. Hansen solubility parameters for the solvents.

Solvent	∂/MPa ½			
	∂_t	∂_d	∂_p	∂_h
o-Xylene	18	17.8	1	3.1
Methanol	29.6	15.1	12.3	22.3
Ethanol	26.5	15.8	8.8	19.4
2,2,2-Trifluoro Ethanol	24.02	15.47	8.3	16.4

Table S4. Calculated interfacial surface energy for NPDI, BHJ, and PUA.

NPDI	E (oxidation)	E (reduction)	Band gap	HOMO	LUMO
Conventional	2.44	−0.78	−3.23	−7.33	−4.10
Coherent Arrangement	2.46	−0.74	−3.21	−7.35	−4.14

Table S5. Photovoltaic parameters for OPVs with a coherent arrangement of NPDI (area: 0.15 cm^2).

	V_{oc} (V)	J_{SC} (mA/cm^2)	$J_{SC,EQE}$ (mA/cm^2)	FF	PCE (%)
C- NPDI	0.728	28.14	25.78	0.59	12.04
A- NPDI	0.789	28.14	26.58	0.65	14.45

Table S6. Electron mobility of electron-only devices containing a coherent arrangement of NPDI interlayer.

	Electron mobility ($cm^2V^{-1}s^{-1}$)
C- NPDI	7.905×10^{-6}
A- NPDI	1.730×10^{-5}

Table S7. Trap density of electron-only devices containing a coherent arrangement of NPDI interlayer.

	V_{TFL}	N_{trap} (# cm^{-3})
C-NPDI	0.918	2.117×10^{16}
A- NPDI	0.731	1.686×10^{16}

Table S8. Photoresponse rate of OPVs with a coherent arrangement NPDI for on/off photocurrent ratios of 0.1 to 0.9.

	τ_{on} (s)	τ_{off} (s)
C-NPDI	1.31 μs	1.25 μs
A- NPDI	1.06 μs	1.22 μs

Table S9. Frequency-dependent responses of OPDs with coherent arrangement of NPDI.

	–3 dB		Variation
	Pristine	**Aged**	
C-NPDI	351 kHz	345 kHz	–1.7%
A- NPDI	445 kHz	442 kHz	–0.6%